Eur. Phys. J. C 54, 61–72 (2008)
DOI 10.1140/epjc/s10052-008-0530-9

THE EUROPEAN PHYSICAL JOURNAL C

Regular Article – Experimental Physics

Search for solar axions emitted in the M1-transition of ^{7}Li* with Borexino CTF

The Borexino Collaboration

G. Bellini[1], J. Benziger[2], S. Bonetti[1], B. Caccianiga[1], F. Calaprice[3], F. Dalnoki-Veress[3], D. D'Angelo[1], H. de Kerret[4], A. Derbin[5,a], A. Etenko[6], K. Fomenko[7], D. Franco[1], C. Galbiati[3], S. Gazzana[8], M.G. Giammarchi[1], M. Goeger-Neff[9], A. Goretti[3], C. Grieb[10], S. Hardy[10], A. Ianni[8], A.M. Ianni[3], M. Joyce[10], V.V. Kobychev[11], G. Korga[8], D. Kryn[4], M. Laubenstein[8], M. Leung[3], E. Litvinovich[6], P. Lombardi[1], L. Ludhova[1], I. Machulin[6], G. Manuzio[12], F. Masetti[13], K. McCarty[3], E. Meroni[1], L. Miramonti[1], M. Misiaszek[14], D. Montanari[8], M.E. Monzani[8], V. Muratova[5], L. Niedermeier[9], L. Oberauer[9], M. Obolensky[4], F. Ortica[13], M. Pallavicini[12], L. Papp[8], L. Perasso[1], R.S. Raghavan[10], G. Ranucci[1], A. Razeto[8], A. Sabelnikov[6], C. Salvo[12], S. Schönert[15], H. Simgen[15], M. Skorokhvatov[6], O. Smirnov[7,b], A. Sotnikov[7], S. Sukhotin[6], Y. Suvorov[8], V. Tarasenkov[6], R. Tartaglia[8], G. Testera[12], D. Vignaud[4], F. von Feilitzsch[9], R.B. Vogelaar[10], M. Wojcik[14], O. Zaimidoroga[7], S. Zavatarelli[12], G. Zuzel[15]

[1] Dipartimento di Fisica Università and INFN Milano, Via Celoria, 16, 20133 Milano, Italy
[2] Department of Chemical Engineering, A-217 Engineering Quadrangle, Princeton NJ 08544-0708, USA
[3] Department of Physics, Princeton University, Jadwin Hall, Washington Rd, Princeton NJ 08544-0708, USA
[4] Astroparticule et Cosmologie APC, 10 rue Alice Domon et Leonie Duquet, 75205 Paris cedex 13, France
[5] St. Petersburg Nuclear Physics Institute, 188300 Gatchina, Russia
[6] RRC Kurchatov Institute, Kurchatov Sq.1, 123182 Moscow, Russia
[7] Joint Institute for Nuclear Research, Joliot Curie 6, 141980 Dubna Moscow region, Russia
[8] INFN Laboratori Nazionali del Gran Sasso, SS 17 bis Km 18+910, 67010 Assergi (AQ), Italy
[9] Technische Universität München, James Franck Strasse, E15, 85747 Garching, Germany
[10] Physics Department, Virginia Polytechnic Institute and State University, Roberson Hall, Blacksburg, VA 24061-0435, USA
[11] Kiev Institute for Nuclear Research, 47 Prospekt Nauki, 06380 Kiev, Ukraine
[12] Dipartimento di Fisica Università and I.N.F.N. Genova, Via Dodecaneso, 33, 16146 Genova, Italy
[13] Dipartimento di Chimica Università di Perugia, Via Elce di Sotto, 8, 06123 Perugia, Italy
[14] M. Smoluchowski Institute of Physics, Jagellonian University, ul. Reymonta 4, 30059 Krakow, Poland
[15] Max-Planck-Institut für Kernphysik, Postfach 103 980, 69029 Heidelberg, Germany

Received: 20 August 2007 /
Published online: 29 January 2008 – © Springer-Verlag / Società Italiana di Fisica 2008

Abstract. Results of background measurements with a prototype of the Borexino detector were used to search for 478 keV solar axions emitted in the M1-transitions of ^{7}Li*. The Compton conversion of axion to a photon $A+e \to e+\gamma$, axioelectric effect $A+e+Z \to e+Z$, decay of axion in two photons $A \to 2\gamma$ and Primakoff conversion on nuclei $A+Z \to \gamma+Z$ are considered. The upper limit on constants of interaction of axion with electrons, photons and nucleons – $g_{Ae}g_{AN} \leq (1.0\text{–}2.4)\times 10^{-10}$ at $m_A \leq 450$ keV and $g_{A\gamma}g_{AN} \leq 5\times 10^{-9}$ GeV^{-1} at $m_A \leq 10$ keV are obtained (90%c.l.). For heavy axions with mass at $100 < m_A < 400$ keV the limits $g_{Ae} < (0.7\text{–}2.0)\times 10^{-8}$ and $g_{A\gamma} < 10^{-9}$–10^{-8} are obtained in assumption that g_{AN} depends on m_A as for KSVZ axion model. These limits are stronger than obtained in previous laboratory-based experiments using nuclear reactor and artificial radioactive sources.

PACS. 14.80.Mz; 29.40.Mc; 26.65.+t

1 Introduction

A natural solution of the strong CP problem was found by Peccei and Quinn by introducing a new global chiral symmetry $U(1)_{PQ}$ [1,2]. Weinberg and Wilczek noted that spontaneous symmetry breaking of $U(1)_{PQ}$ at energy $\sim f_A$ leads to existence of a new neutral spin-zero pseudoscalar particle -axion [3,4]. The original PQWW- or standard axion model assumed that f_A is equal to electroweak scale: $f_A = (\sqrt{2}G_F)^{-1/2} \approx 250$ GeV. The standard axion mass depends on the number of quark doublets N and unknown

[a] e-mail: derbin@pnpi.spb.ru
[b] e-mail: osmirnov@jinr.ru

parameter X, which is the ratio of two Higgs vacuum expectation values: $m_A(\text{keV}) \approx 25N(X + 1/X) \geq 150\,\text{keV}$. This model was excluded after extensive experimental searches for the standard axion (see [5] and refs therein).

New axion models decoupled the scale of PQ symmetry breaking from the electroweak scale and extended value of f_A up to the Plank mass $\approx 10^{19}$ GeV. Two types of model for the invisible axion have been developed: the Kim–Shifman–Vainstein–Zakharov model (KSVZ or hadronic axion) [6, 7] and the Dine–Fischler–Srednicki–Zhitnitski model (DFSZ or GUT axion models) [8, 9]. The strength of the axion's couplings to photon, electron and nucleons is given by effective coupling constants $g_{A\gamma}$, g_{Ae}, g_{AN}. Since the elementary axion couplings are model dependent, these effective couplings are model dependent as well. The interaction strength scales as f_A^{-1}, but also includes significant uncertainties from model-dependent numerical parameters. In contrast to the DFSZ axions, KVSZ axions have no coupling to leptons and ordinary quarks at the tree level, which results in strong suppression of the interaction of KVSZ axion with electrons through radiatively induced coupling. Moreover, in some models axion photon coupling may differ from the original DFSZ or KVSZ $g_{A\gamma}$ couplings by a factor less then 10^{-2}.

While laboratory-based experiments exclude DFSZ- and KSVZ-axions with masses above a few eVs, astrophysical and cosmological arguments exclude practically all region of possible values of axion's masses leaving the ranges of about 10^{-6}–10^{-2} eV (see [5, 10] and refs. therein).

New possibilities for solving the strong CP-problem based on the concept of mirror world particle [11] and on sypersymmetric extension of the standard model [12] were suggested. In these models the axions with mass about ~ 1 MeV or above are not excluded by the present experimental and astrophysical limits. Because, besides solving the strong CP problem, the axion provides also a well motivated candidate for at least a part of the non-baryonic dark matter, experimental efforts to detect axions are still intensively continued.

If axions exist, the Sun would be an intense source of these particles. Axions can be efficiently produced in the Sun by Primakoff conversion of photons in the electric field of the plasma. The resulting axion flux has an average energy of about 4 keV and can be detected by inverse Primakoff conversion in laboratory magnetic fields [13–22] or by the coherent conversion to photons in crystal detectors [23–25].

Because of the axion coupling to nucleons there is another component of solar axions emitted in nuclear magnetic transitions of excited nuclei. The temperature in the center of the Sun is ~ 1.3 keV and some nuclei (e.g. ^{57}Fe, ^{55}Mn) having low-laying nuclear levels can be excited thermally [26]. These axions can be detected via resonant absorption in nuclear targets [27–29]. The probability of emission and subsequent absorption of the axion in a magnetic transition is determined only by the axion–nucleon coupling.

The other source of axions are reactions of the solar cycle that produce solar energy. Figure 1 shows the scheme of electron capture $^7\text{Be} + e^- \rightarrow {}^7\text{Li}^* + \nu_e$ [30]. The 478 keV

Fig. 1. Electron capture decay scheme of ^{7}Be [30]

excited state of ^{7}Li is a short-lived intermediate state following electron capture with branching ratio $\eta = 0.105$. Since axions are pseudoscalar particles they can be emitted in M1-transitions from the first excited state to the groundstate. Except for in-flight decay and interaction in the Sun, the flux of solar axions at the Earth is defined by the electron capture rate of ^{7}Be to the first excited state of ^{7}Li, which is given by the standard solar model. The ^{7}Be electron capture also produces neutrinos with a flux equal to $4.8 \times 10^9(\pm 10\%)\nu/(\text{cm}^2\,\text{s})$ at the Earth [31]. The expected flux of axions is directly related to the total flux of ^{7}Be neutrino and is comparable with axion flux in experiments using nuclear reactors [32] or artificial radioactive sources [33] (see [5] and refs. therein). An attempt to detect such axions through resonant absorption in ^{7}Li nuclei target have been performed in [34, 35].

In this letter we present the results of a search for solar axions emitted in the 478 keV transition in ^{7}Li following the electron capture decay of ^{7}Be. Detection limits of axions are based on axion interactions with electrons by Compton axion to photon conversion $A + e \rightarrow e + \gamma$ and the axioelectric effect $A + e + Z \rightarrow e + Z$, using the prototype of the Borexino detector. The amplitudes of these processes are defined by g_{Ae} coupling. We also consider the possible signals from the decay of the axion into two γ-quanta and from Primakoff conversion on nuclei $A + Z \rightarrow \gamma + Z$. The amplitudes of these reactions depend on axion-photon coupling $g_{A\gamma}$. The signature of all above reactions is the appearance of 478 keV peak in the energy spectra of CTF. The extremely low background level of natural radioactivity and the large mass of the CTF allowed setting new limits on the electron, neutrino and nucleon stability, neutrino electromagnetic properties and violation of the Pauli exclusion principle [36–41].

2 Axion interactions

2.1 Axion–nucleons coupling: axion emission in the nuclear magnetic transitions

The coupling of the axion field ϕ_A to the nucleon is defined by the isoscalar (g^0_{AN}) and isovector axion–nucleon (g^3_{AN})

coupling constants:

$$L = i\overline{\psi_N}\gamma_5 \left(g^0_{AN} + g^3_{AN}\tau_3\right)\psi_N\phi_A\,. \quad (1)$$

In the KSVZ axion model the dimensionless coupling constants g^0_{AN} and g^3_{AN} are related to f_A by expressions [42, 43]:

$$g^0_{AN} = \frac{m_N}{6f_A}\left[2S + (3F - D)\frac{1+z-2w}{1+z+w}\right] \quad (2)$$

and

$$g^3_{AN} = \frac{m_N}{2f_A}\left[(D+F)\frac{1-z}{1+z+w}\right], \quad (3)$$

where z and w are ratios of u-, d- and s-quark masses $z = m_u/m_d \cong 0.56$, $w = m_u/m_s \cong 0.029$ and $M_N \approx 939\,\mathrm{MeV}$ is the nucleon mass. Axial-coupling parameters F and D are obtained from hyperon semi-leptonic decays with high precision: $F = 0.462 \pm 0.011$, $D = 0.808 \pm 0.006$ [44]. The parameter S characterizing the flavor singlet coupling is still a poorly constrained parameter. Its value changes from $S = 0.68$ in the naive quark model down to $S = -0.09$ which is given on the basis EMC collaboration measurements [45]. As a result the value of the sum $(g^0_{AN} + g^3_{AN})$ is determined within a factor of two. We will use $S = 0.4$ [46] as reference when we calculate axion flux for KSVZ axion model.

The axion mass (in eV units) is given in terms of f_A by

$$m_A = \frac{f_\pi m_\pi}{f_A}\left(\frac{z}{(1+z+w)(1+z)}\right)^{1/2} \approx \frac{6.0\times10^6}{f_A(\mathrm{GeV})}\,. \quad (4)$$

Numerical values of g^0_{AN} and g^3_{AN} are related to the hadronic axion mass:

$$g^0_{AN} = -3.50\times10^{-8}(m_A/1\,\mathrm{eV})\,, \quad (5)$$

$$g^3_{AN} = -2.75\times10^{-8}(m_A/1\,\mathrm{eV})\,. \quad (6)$$

The axion-to-gamma decay branching ratio (ω_A/ω_γ) of the M1 transition calculated in the long-wavelength limit is given by the expression [26, 33]:

$$\frac{\omega_A}{\omega_\gamma} = \frac{1}{2\pi\alpha}\left[\frac{p_A}{p_\gamma}\right]^3 \frac{1}{1+\delta^2}\left[\frac{g^0_{AN}\beta + g^3_{AN}}{(\mu_0 - 0.5)\beta + \mu_3 - \eta}\right]^2, \quad (7)$$

where $\alpha \cong 1/137$ is the fine structure constant, p_A and p_γ are the momenta of the axion and the photon, and $\mu_0 = 0.88$ and $\mu_3 = 4.71$ are the isoscalar and isovector magnetics moments. The η and β are two nuclear-structure dependent ratios and δ is $E2/M1$ mixing ratio for the nuclear transition. For 478 keV M1-transition of ^{7}Li $\delta \cong 0.005\%$ and $\eta \cong 0.5$ and $\beta \cong 1$. For given parameters the branching ratio can be rewritten as:

$$\frac{\omega_A}{\omega_\gamma} = 1.03\left(g^0_{AN} + g^3_{AN}\right)^2 (p_A/p_\gamma)^3\,. \quad (8)$$

From (7), (5) and (6) one can obtain the ratio ω_A/ω_γ as a function of axion mass:

$$\frac{\omega_A}{\omega_\gamma} = 4.02\times10^{-15} m_A^2 (p_A/p_\gamma)^3\,, \quad (9)$$

where m_A is expressed in eV units. The probability of axion emission increases as m_A^2, reaches maximum at $m_A = (2/5)^{1/2}p_\gamma$ and decreases at larger masses because of $(p_A/p_\gamma)^3$ factor. The expected solar 478 keV axion flux equals:

$$\Phi_{A0} = \eta\Phi_\nu(^7\mathrm{Be})(\omega_A/\omega_\gamma)\,. \quad (10)$$

The values of g^0_{AN} and g^3_{AN} for the DFSZ axion depend on additional unknown parameter $\cos^2\beta$ which is defined by the ratio of the Higgs vacuum expectation values. For the case of ^{7}Li transition the ratio $(\omega_A/\omega_\gamma)^{\mathrm{DFSZ}}$ lies in the interval $\sim (0.1\text{–}2.0)(\omega_A/\omega_\gamma)^{\mathrm{KSVZ}}$. The lower and upper bounds of the interval are defined by values $\cos\beta = 0, 1$ respectively.

Because the branching ratio (ω_A/ω_γ) is model dependent we can consider parameter $(g^0_{AN} + g^3_{AN})^2$ in the expression (8) as a free unknown parameter characterizing axion–nucleon coupling. The value $(g^0_{AN} + g^3_{AN})^2$ is close to $(g_{AN})^2 = ((g^0_{AN})^2 + (g^3_{AN})^2)$ usually defined as a measure of the total coupling [47].

2.2 Axion–electron coupling: Compton conversion of axion to photon $A + e \to \gamma + e$ and axioelectric effect $A + e + Z \to e + Z$

The coupling of the axion to the electron is governed by the Lagrangian:

$$L = ig_{Ae}\overline{\psi_e}\gamma_5\psi_e\phi_A\,, \quad (11)$$

where g_{Ae} is a dimensionless Yukawa coupling constant. The parameter g_{Ae} is associated with mass of the electron m, so that $g_{Ae} = C_e m/f_A$, where C_e is a model dependent factor of the order of unity. In the standard PQWW-axion model the values $f_A = 250\,\mathrm{GeV}$, $C_e = 1$ are fixed and $g_{Ae} \approx 2\times10^{-6}$. In DFSZ-axion models $C_e = 1/3\cos^2\beta$, where β is an arbitrary angle. If one set $\cos^2\beta = 1$ the axion–electron coupling is related to axion mass as $g_{Ae} = 2.8\times10^{-11}m_A$, where m_A is expressed in eV units.

The hadronic axion has no tree-level couplings to the electron, but there is an induced axion–electron coupling at the one-loop level [42]:

$$g_{Ae} = \frac{3\alpha^2 Nm}{2\pi f_a}\left(\frac{E}{N}\ln\frac{f_A}{m} - \frac{2}{3}\frac{4+z+w}{1+z+w}\ln\frac{\Lambda}{m}\right), \quad (12)$$

where N and E are the model dependent coefficients of the electromagnetic and color anomalies, $\Lambda \approx 1\,\mathrm{GeV}$ is the cutoff at the QCD confinement scale. The interaction strength of the hadronic axion with the electron is suppressed by a factor $\sim\alpha^2$. The numerical value of g_{Ae} for $E/N = 8/3$, which is characteristic of GUT models, and for $N = 1$ is $g_{Ae} = 2.2\times10^{-15}\left(\frac{8}{3}\ln\left(\frac{1.2\times10^{10}}{m_A}\right) - 14.6\right)m_A$, where m_A is expressed in eV units.

The axion can scatter an electron to produce a photon in the Compton-like process $A + e \to \gamma + e$. The Compton differential cross section for electrons was calculated

in [32, 33, 49]:

$$\frac{\mathrm{d}\sigma}{\mathrm{d}\Omega} = \frac{g_{Ae}^2 \alpha E_\gamma}{8\pi m^2 p_A} \times \left[1 + \frac{4m^2 E_\gamma^2}{y^2} - \frac{4mE_\gamma}{y} - \frac{4m_A^2 p_A^2 m E_\gamma}{y^3} \sin^2\theta\right], \quad (13)$$

where E_γ is the energy of γ-quanta, p_A and E_A are the momenta and the energy of the axion respectively, θ is the angle between the axion and emitted photon and $y = 2mE_A + m_A^2$. The spectra of γ-quanta calculated for different axion mass are shown in Fig. 2. The energy spectra of electrons can be found from relation $E_e = E_A - E_\gamma$, where $E_A \cong 477.6$ keV is the energy of nuclear transition.

The integral cross section corresponding to this mode is [32, 33, 49]:

$$\sigma_{\mathrm{CC}} = \frac{g_{Ae}^2 \alpha}{8m^2 p_A} \left[\frac{2m^2(m+E_A)y}{(m^2+y)^2} + \frac{4m\left(m_A^4 + 2m_A^2 m^2 - 4m^2 E_A^2\right)}{y(m^2+y)} + \frac{4m^2 p_A^2 + m_A^4}{k_a y} \ln\frac{m+E_A+p_A}{m+E_A-p_A}\right]. \quad (14)$$

The cross sections calculated for PQWW-, DFSZ- and KSVZ-axions as a function of axion mass are shown in Fig. 3. For the standard axion g_{Ae} is fixed as $g_{Ae} = m/250$ GeV and does not depend on axion mass, for DSFZ original model $g_{Ae} = m/3f_A = 2.8 \times 10^{-11} m_A(\mathrm{eV})$ and for the hadronic axion g_{Ae} was calculated according to the formula (12). As one can see from the curve (1) for standard axion with fixed g_{Ae}, the phase space contribution to the cross section is approximately independent of m_A and for $m_A < 200$ keV is $\sigma_{\mathrm{CC}} \approx g_{Ae}^2 \times 5.5 \times 10^{-25}$ cm^2.

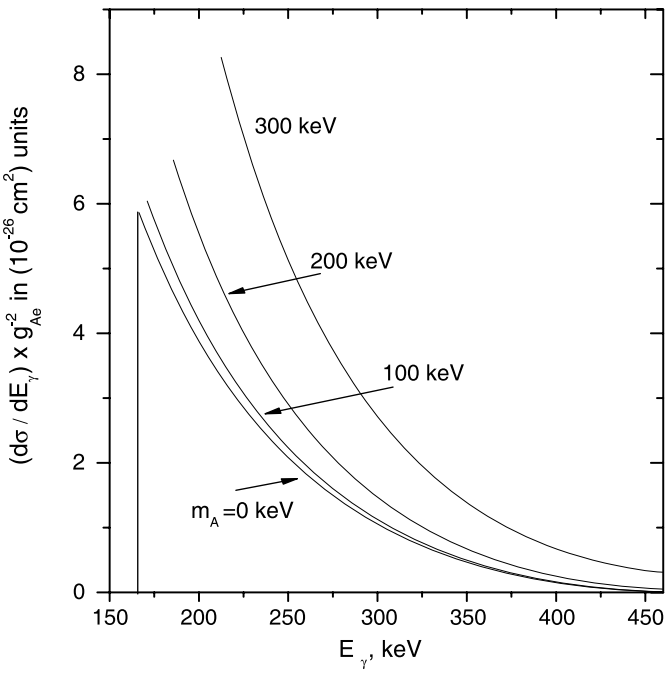

Fig. 2. Spectra of γ-quanta from axion Compton conversion $A + e \to \gamma + e$ calculated for different axion masses

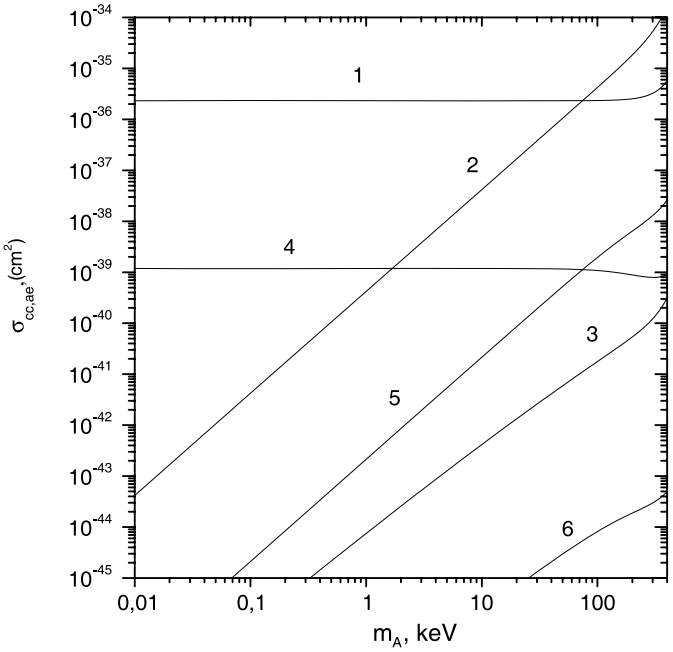

Fig. 3. The cross sections Compton conversion of axion to photon (*lines* 1, 2, 3) and axioelectric effect (*lines* 4, 5, 6) cross sections for ^{12}C are given as a function of axion mass m_A for different axion–electron coupling: 1 – standard PQWW axion, 2 – DFSZ axion with $\cos^2\beta = 1$, 3 – KSVZ or hadronic axion

The 90% of reactions $^7\mathrm{Be} + e^- \to {}^7\mathrm{Li}^* + \nu_e$ occur within 0.11 radiuses of the Sun [50]. Axions leaving the center of the Sun pass through the matter layer with $\approx 6.8 \times 10^{35}$ electrons/cm^2. As the result the absorption of the axions due to Compton process is lower than 10%, if $g_{Ae} \leq 5 \times 10^{-7}$. DFSZ axions of mass $m_A \leq 20$ keV would escape from the Sun with insignificant absorption. The resonant absorption of 478 keV axions by ^{7}Li nuclei is the other possible reaction in which axion can disappear, but because of low abundance of lithium in the Sun the probability of such process is less than 10^{-4}.

The other process associated with axion–electron coupling is the axio-electric effect $A + e + Z \to e + Z$ (the analogue of the photo-electric effect). In this process the axion disappears and an electron is emitted from an atom with energy of the absorbed axion minus the electron binding energy E_b. The cross section of axio-electric effect on K-electrons for axion energy $E_A \gg E_\mathrm{b}$ was calculated in [49]:

$$\sigma_{\mathrm{AE}} = 2(Z\alpha m)^5 \frac{g_{Ae}^2}{m^2} \frac{p_e}{p_A} \frac{4E_A(E_A^2 + m_A^2)}{\left(p_A^2 - p_e^2\right)^4} - \frac{2E_A}{\left(p_A^2 - p_e^2\right)^3} - \frac{64}{3} p_e^2 p_A^2 m \frac{m_A^2}{\left(p_A^2 - p_e^2\right)^6} - \frac{16 m_A^2 p_A^2 E_e}{\left(p_A^2 - p_e^2\right)^5} - \frac{E_A}{p_e p_A} \frac{1}{\left(p_A^2 - p_e^2\right)^2} \ln\frac{p_e + p_A}{p_e - p_A}. \quad (15)$$

The cross section (15) has a Z^5 dependence and for carbon atoms the cross section is $\sigma_{\rm AE} \approx g_{Ae}^2 \times 2.8 \times 10^{-28}\,{\rm cm}^2$/ electron. This value is about 3 orders of magnitude lower than for axion Compton conversion. However, taking into account the different energy dependence ($\sigma_{\rm CC} \sim E_A$, $\sigma_{\rm AE} \sim (E_A)^{-3/2}$) and Z^5 dependence, the axio-electric effect can be more effective to search for low energy axions with detectors having high Z. Because of the low abundance of heavy elements (with $Z \geq 50$) in the Sun (~ 1 ppb atom/atom), the probability of axio-electric absorption of 478 keV axion inside the Sun is less than 10^{-7}. The abundance of Fe atoms constrains $g_{Ae} < 1.1 \times 10^{-4}$, in this case 90% of axions escape from the Sun. The cross sections of axio-electric effect calculated according to (15) for three variants of axion models, are shown in Fig. 3.

2.3 Axion–photon coupling: axion decay $A \to 2\gamma$ and the Primakoff production on carbon nuclei $A + {}^{12}{\rm C} \to \gamma + {}^{12}{\rm C}$

The Lagrangian for the interaction of the axion with the photons is:

$$L = -(1/4) g_{A\gamma} F^{\mu\nu} \tilde{F_{\mu\nu}} \phi_A = g_{A\gamma} \mathbf{E} \cdot \mathbf{B} \phi_{\mathbf{A}}\,, \qquad (16)$$

where F is electromagnetic tensor and $g_{A\gamma}$ is an axion–photon coupling constant with dimension of (energy)$^{-1}$ which is usually presented as:

$$g_{A\gamma} = \frac{\alpha}{2\pi f_A}\left(\frac{E}{N} - \frac{2(4+z+w)}{3(1+z+w)}\right) = \frac{\alpha}{2\pi f_A} C_{A\gamma\gamma}\,, \qquad (17)$$

where E/N is a model dependent parameter of the order of unity. $E/N = 8/3$ in DFSZ axion models ($C_{A\gamma\gamma} = 0.74$) and $E/N = 0$ for original KSVZ axion ($C_{A\gamma\gamma} = -1.92$). The value of the second term inside brackets is 1.95 ± 0.08 and axion–photon coupling may be significantly reduced in axion models in which E/N is close to 2 [43].

With this axion–photon coupling, axion decays into two photons with the lifetime:

$$\tau_{\rm c.m.} = \frac{64\pi}{g_{A\gamma}^2 m_A^3}\,. \qquad (18)$$

The phase space for decay depends on m_A^3. For $\tau_{\rm c.m.}$ measured in seconds, $g_{A\gamma}$ – in GeV^{-1} and m_A – in eV one obtains:

$$\tau_{\rm c.m.} = 1.3 \times 10^5 g_{A\gamma}^{-2} m_A^{-3} = 3.5 \times 10^{24} m_A^{-5} C_{A\gamma}^{-2}\,. \qquad (19)$$

The axion emitted in the Sun can decay on its flight to the Earth. Because of axion decay the sensitivity of the search drops off for large values of $g_{A\gamma}^2 m_A^3$. The flux of axions reaching the detector is given by expression:

$$\Phi_A = \exp\left(-\frac{\tau_{\rm f}}{\tau_{\rm c.m.}}\right)\Phi_{Ao}\,, \qquad (20)$$

where Φ_{A0} is original axion flux (10), $\tau_{\rm c.m.}$ defined by (19) and $\tau_{\rm f}$ is the time of flight in c.m.s.:

$$\tau_{\rm f} = \frac{m_A}{E_A}\frac{L}{\beta c}\,. \qquad (21)$$

Here $L = 1.5 \times 10^{13}$ cm is the average distance between Sun and Earth and $\beta = p_A/E_A$.

The number of $A \to \gamma\gamma$ decays in detector of volume V is:

$$N_\gamma = \Phi_A \frac{\omega_A}{\omega_\gamma}\frac{V m_A}{\beta c E_A \tau_{\rm c.m.}}\,. \qquad (22)$$

Function N_γ calculated for KSVZ model is shown in Fig. 4 for different values of m_A. The maximum N_γ corresponds to $m_A = ((8/6)\tau_{\rm c.m.} m_A^5/(\tau_{\rm f}/m_A))^{1/6} = 45$ keV, where $\tau_{\rm c.m.}$ and $\tau_{\rm f}$ are defined by (19) and (21). The experiment is not so sensitive to low m_A (due to the low probability of axion decay) as for the high values of m_A, because in this case axion decays during its flight from the Sun.

Another process depending on $g_{A\gamma}$ coupling is the Primakoff photoproduction on carbon nuclei $A + {}^{12}{\rm C} \to \gamma + {}^{12}{\rm C}$. The integral Primakoff conversion cross section is [33]:

$$\sigma_{\rm PC} = g_{A\gamma}^2 \frac{Z^2\alpha}{2}\left[\frac{1+\beta^2}{2\beta^2}\ln\left(\frac{1+\beta}{1-\beta}\right) - \frac{1}{\beta}\right]\,. \qquad (23)$$

Because the cross section depends on $g_{A\gamma}$ coupling, the decrease of axions flux due to $A \to 2\gamma$ decays during their flight from the Sun, should be taken into account. The

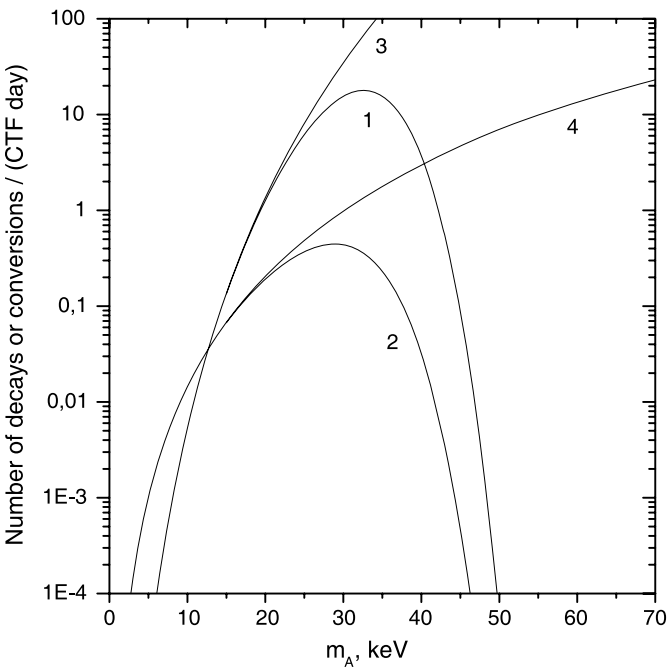

Fig. 4. The expected number of axion decays (l) and Primakoff conversion (2) in CTF volume per day for KSVZ axion model. *Lines* (3) and (4) are calculated for above reactions in assumption that the axion does not decay in its flight from the Sun

axion flux at the detector was calculated by the method described above. The atomic-screening corrections for ^{12}C were introduced in accordance to the method proposed in [33]. The expected number of Primakoff conversions calculated for the CTF detector in accordance to (23) and (20) are shown in Fig. 4. Because of a loss of axions due to Primakoff conversion on protons inside the Sun, the sensitivity of the search is restricted to $g_{A\gamma} < 1 \times 10^{-4}\,\mathrm{GeV}^{-1}$, corresponding to DFSZ axion masses less then 0.7 MeV .

3 Borexino CTF

Borexino, a real-time detector for low energy neutrino spectroscopy, will soon start the taking data at the underground laboratory at Gran Sasso (for detailed description of the detector see [51] and references therein). The main goal of the detector is the direct measurement of the solar ^{7}Be neutrinos flux of all flavours via neutrino-electron scattering in an ultra-pure liquid scintillator (LS). The prototype of the Borexino detector – counting test facility (CTF) – was constructed with the aim to test the key concepts of Borexino, namely the possibility to purify a large mass of liquid scintillator at the level of contamination for U and Th of $\sim 10^{-16}$ g/g. CTF is a simplified scaled version of the Borexino detector. Its active volume, ~ 4 tons of liquid scintillator, is contained in a transparent spherical nylon vessel, 2 m diameter and 0.5 mm thick. The active detector is surrounded by 100 PMTs mounted on an open support structure. The PMTs are fitted with light concentrators which provide a 21% optical coverage. The construction is immersed in 1000 m^3 of high purity shielding water, contained in an external cylindrical tank 10 m diameter and 11 m high. Water shields the scintillator against γ radiation emitted by radioactive contaminants in the PMTs and their support structure as well as against γ's following the capture of neutrons generated within the walls of the experimental hall. Another 16 upward-looking PMTs mounted on the bottom of the tank form an active muon veto system (MVS). They detect the Cherenkov light of muons that cross the water without intersecting with the scintillator. The muon-veto was tuned to maximize the muon tagging efficiency while minimizing the probability of scintillation light pickup for sub MeV events (CTF was optimized to study backgrounds in the $[0.25, 0.8]$ MeV energy range, where Borexino will look for ^{7}Be solar neutrino interactions [51]). A more detailed description of the CTF detector can be found in [52–56].

The electronics of CTF are designed to record fast delayed coincidences without appreciable dead time. Time and charge information of the PMT pulses of an event are recorded by a set of ADCs and TDCs (group 1 chain). During the acquisition time, a second set of ADCs and TDCs (group 2 chain) is sensitive to a possible other event occurring within 8.3 ms. The coincidence time between the two chains is measured by means of a long range TDC. Subsequent events are ignored until the group 1 chain is ready again. The group 1 trigger is fired when 6 PMT hits occur within a window of 30 ns. The corresponding energy threshold is measured to be ~ 20 keV at 50% detection efficiency; 99% detection efficiency corresponds to 90 keV energy release in the scintillator. The energy response of the detector is calibrated run-by-run, using the light yield obtained by fitting the ^{14}C energy spectrum: on average ~ 3.8 photoelectrons (p.e.) per PMT are detected for a 1 MeV recoiling electron at a random position within the detector volume. Electronics of each channel from the PMT to the ADC is linear up to 20 p.e., which guarantees a linear energy response for events below 4.5 MeV.

The CTF has been in operation since 1993. During the 1993–1995 campaign (CTF1), the detector was filled with ~ 4 tons of pseudocumene (PC, 1,2,4-trimethylbenzene, $C_6H_3(CH_3)_3$, $\rho = 0.88\,\mathrm{g/cm^3}$) to which PPO (2,5- Diphenyloxazole, $C_{15}H_{11}NO$) was added as a wavelength shifter in low concentration (1.5 g/l). This campaign was focused on studying backgrounds for the Borexino scintillator [52]. In 1999, CTF was run again (CTF2), this time with PXE (1-Phenyl-1-xylylethane, $C_{16}H_{18}$, $\rho = 0.995\,\mathrm{g/cm^3}$) scintillator. It was upgraded to include an active muon-veto; also, a second, 125 micron thick nylon membrane was added in the water space between the PMTs and the scintillator, aiming to suppress Rn diffusion from the periphery to the center of the detector [53]. These two additions turned CTF into a sensitive detector in the field of rare events physics, as proven by the results in [36–39, 41]. In 2002 a third campaign with $PC + PPO$ liquid scintillator began (CTF3); it is still in progress to finalize the purification strategy for the Borexino scintillator.

The mass of the scintillator (3.75 tons) was defined by measuring the buoyancy with a precision of 5%. The total time of data taking in CTF3 is more than 800 days, the dead time of the electronics introduces an inefficiency of $\simeq 12\%$ for the observed counting rate (about 1 cps). The measurements were performed in ~ 24 h runs. The end-point of ^{14}C β-spectrum was used to check the energy calibration stability. No systematic shift in energy scale with time has been found, the slow varying corrections to the energy scale were obtained using the position of the end-point of ^{14}C β-spectrum. The scintillator fastest light decay component time is less than 5 ns which provides good position reconstruction. The precision of the spatial reconstruction of the detector was defined using sources inserted at different positions inside the active volume, and was found to be ≈ 10 cm (1σ) at ≈ 0.8 MeV (from 7.8 MeV α-events of ^{214}Po (tagged by ^{214}Bi-^{214}Po delayed coincidence).

In the present study we use CTF3 data collected during 623 days of data taking (corresponding to 548 days of live-time) to search for possible axion signature. The first period of the data taking of about 200 days was excluded from the analysis because of the presence of a strong α-peak from ^{210}Po in the region of interest.

4 Data selection and analysis

The energy calibration of the first group of the electronics was performed using ^{14}C events and checked at higher energies using the first event of the delayed ^{214}Bi-^{214}Po coin-

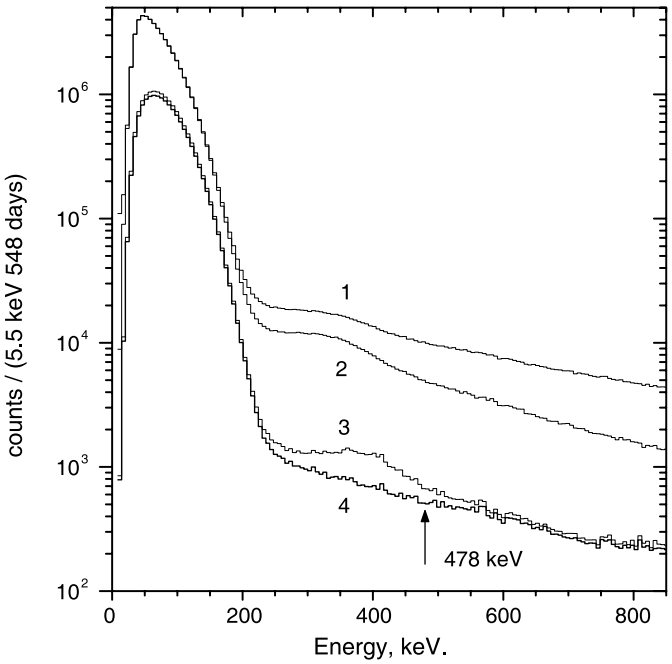

Fig. 5. CTF3 spectrum measured during 548 days. The sequence of the applied cuts is shown from *upper plot* to the *lower one*: 1 – total data; 2 – data without events tagged by muon veto and time correlated events; 3 – radial cut $r < 83$ cm; 4 – all previous cuts plus α/β discrimination

cidences (originating from ^{222}Rn in the LS); ^{214}Bi β decays with Q value of 3.2 MeV. The energy and spatial resolution of the CTF3 detector are very close to those of CTF1 [52, 58].

In our analysis we used the data collected with the CTF3 detector during 548 days of data taking (see Fig. 5). The spectrum without any cut applied is presented on the top. The next spectrum is obtained excluding events tagged by the muon veto and time-correlated events (that occurred in the time window $\Delta t < 8.2$ ms). The muon veto suppresses the background rate by up to two orders of magnitude, depending on the energy region. On the next stage a cut on the reconstructed radius is applied, aiming to remove the surface background events and leave the events uniformly distributed over the detector's volume. The selected value of parameter $R = 85$ cm for the spatial cut corresponds to maximum signal/background ratio. The efficiency of the radial cut has been simulated using MC method taking into account the dependence of the spatial reconstruction precision on energy and position. The obtained value of efficiency for γ-quanta with energy 478 keV is $\varepsilon_R(85) = 0.65$. Additional α/β discrimination was applied to eliminate contribution from α particles (lower spectrum in Fig. 5). The α/β discrimination removes the majority of α's (which are mainly 5.5 MeV α-particles from ^{210}Po decay, corresponding to an electron energy release of ~ 380 keV) while leaving (80–95)% of β's and γ's at 700–800 keV energies (depending on the value of parameter of α/β discrimination). The value of $\epsilon_{\alpha/\beta}$ slightly increases with decrease of an energy. The limits obtained in further analysis uses the value of $\epsilon_{\alpha/\beta}(700\,\text{keV})$ in order to provide correct limit estimation.

During the data taking which continued for more than 3 years some of the PMTs were broken. In order to equalize the charge scale for different runs, it was first corrected for the number of PMTs in operation (using the first run as a reference) and only then the fine calibration on the base of ^{14}C β-spectrum described above was applied.

After these cuts, we estimate that the internal background (due to the internal contamination of PC with natural radioactive isotopes) of CTF3 is about $0.08\,\text{keV}^{-1}\cdot\text{t}^{-1}\cdot\text{day}^{-1}$ at 500 keV.

5 Simulation of the CTF3 response function and fitting procedure

The Monte Carlo method has been used to simulate the CTF response $S(E)$ to electrons and γ-quanta appearing in axion interactions. The gamma-electron showers were followed using the EGS-4 code [57], taking into account the effect of ionization quenching and the dependence of the registered charge on the distance from the detector's center.The axion events were assumed to be uniformly distributed in the whole volume of the liquid scintillator and in 1 m water layer close to the LS. The spatial reconstruction was simulated in order to take into account the spatial cut applied.

The total number of events to simulate was divided into time periods corresponding to the different number of PMTs in operation, the simulation was performed and then the procedure of the scale equalization used with the real data was applied to the MC data for each period. The simulated response corresponds to the sum of the contributions over all periods.

The energy of initial electrons and γ-quanta appearing in axion Compton conversion were generated according to the cross section (13) shown on Fig. 2. The responses for the axion decay in two γ quanta in the liquid scintillator and in the water shield were calculated taking into account the angular correlation between photons. The response functions for axion Compton conversion $S_{\text{CC}}(E)$ (electron and γ-quanta with sum energy of 478 keV), for axio-electric effect S_{AE} (electron with energy 478 keV), axion decay $S_{2\gamma}(E)$ (two γ-quanta with energy 239 keV) and for Primakoff conversion $S_{\text{PC}}(E)$ (478 keV γ-quanta) are shown in Fig. 6. Response functions S_{CC}, S_{AE}, $S_{2\gamma}$ and S_{PC} are normalized to 1 axion interaction in liquid scintillator. The shift in the position of the total absorption peak for corresponding γ's is caused by the so called ionization quenching effect (see i.e. comments in [36]) leading to the nonlinearity of the amount of emitted light with respect to the electron energy. Response function $S_{2\gamma\text{ext}}$ ($A \to 2\gamma$ decay in water) is normalized to one decay in the CTF volume. S_{PCext} response was simulated for Primakoff photoproduction on ^{16}O nuclei taking into account the difference in densities of water and liquid scintillator. Additional shift in position for the external γ is due to the fact that this interactions occur mainly in the surface layer, where the light collection is suppressed by the total reflection effect on the scintillator/water interface (index of refraction of

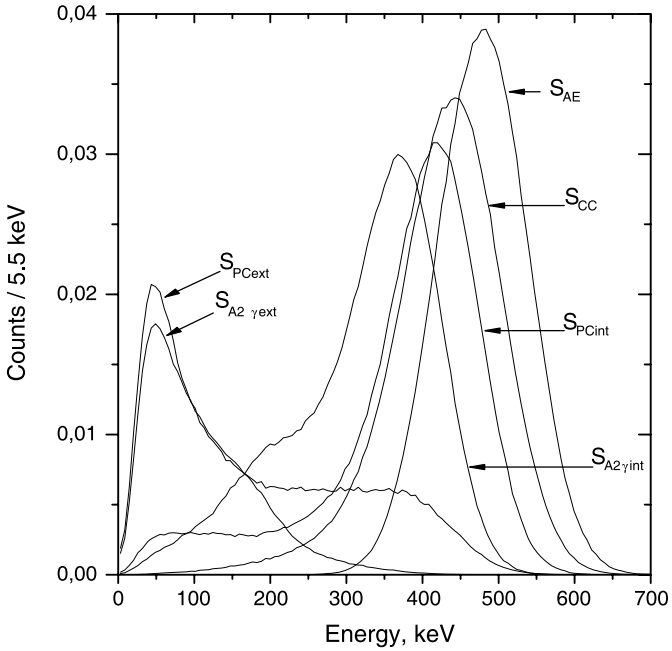

Fig. 6. Simulated responses to axion interactions in CTF (no radial cut applied). $S_{\rm AE}$ – axio-electric effect (477 keV electrons), $S_{\rm CC}$ – Compton axion to photon conversion (electron and γ-quanta), $S_{\rm PCint}$, $S_{\rm PCext}$ – Primakoff conversion (478 keV γ-quanta in LS and in water), $S_{A2\gamma{\rm int}}$, $S_{A2\gamma{\rm ext}}$ – decay $A \to 2\gamma$ in LS and in water shield, consequently

PC is $n \approx 1.5$). More details on the MC simulation of the CTF detector can be found in [40].

The energy of an event in the CTF detector is defined using the total collected charge from all PMTs. The coefficient linking the event energy and the total collected charge is called light yield. The study with the radioactive sources placed at the different positions inside the CTF inner vessel showed that the CTF response can be approximated by a Gaussian, with sigma defined by the following formula [36, 58]:

$$\sigma_Q = \sqrt{(1+\overline{v_1})Q + v_p Q^2}\,, \qquad (24)$$

where Q is the mean total registered charge for the events of energy E distributed over the detector's volume; v_1 is the relative variance of the PMT single photoelectron charge spectrum (it was defined with a high precision during PMT acceptance test: $\overline{v_1} = 0.34$). The parameters v_p give additional signal variance arising from the following reasons: (1) additional variance for the source distributed over the detector's volume in comparison to the point-like source at the detector's center (detector's spatial non-uniformity); (2) uncertainties of the procedure of the charge scale equalization: $Q_{\rm eq} = Q_{\rm reg} * {\rm scale}$ (scale takes into account calibration corrections) yields another member of the form $c \times Q^2$ in formula (24); (3) the same kind of member arises from an intrinsic scintillator resolution. There is no need to keep these additive parameters apart, so in the model we used the only parameter v_p.

The total experimental spectrum (see curve 4 in Fig. 5) is well described with the sum of the ^{14}C β-spectrum smeared by the resolution (24) and an exponential function. The end-point energy of the ^{14}C spectrum is known from experiments with high accuracy $E_0 = (156 \pm 0.5)$ keV, and was fixed in the calculations. This parameter is in strong correlation with the light yield A, and its uncertainty is masked by the uncertainty in the parameter A. The model function has 5 free parameters: the number of ^{14}C events, light yield A, parameter describing detector's nonuniformity v_p and 2 parameters of the exponential function. Ionization quenching $k_{\rm B} = 0.017\,{\rm cm}^{-1}\,{\rm MeV}^{-1}$ and C^{14} shape factor $\alpha = -0.7\,{\rm MeV}^{-1}$ (corresponding to the parameterization of the shape factor in the form $f(E) = 1 + \alpha E$) were fixed at their best-fit values. More details on the CTF experimental spectrum fitting procedure can be found in [36, 37]. The energy scale in the fit is defined with a precision of $< 2\%$. The deviation of the model from experimental data without radial cut has pure statistical origin ($\chi^2/{\rm n.d.f.} \simeq 1.0$).

The influence of the radial cut on the uniformly distributed events was studied using MC data and checked on the experimental data. The radial cut has a weak dependence on the energy and was described by a simple two-parametric approximation for every value of the radial cut. The parameters of the approximation were defined with ^{14}C energy region and were fixed in the later analysis, the slow-varying function in the region of interest has no influence on the final result.

The upper limit on the possible admixture of axion interactions in the detector was established adding the corresponding response function ($S_{\rm CC}(E)$, $S_{\rm AE}(E)$, $S_{2\gamma}(e)$, $S_{\rm PC}(E)$) to the model. The ^{14}C spectrum allows to de-

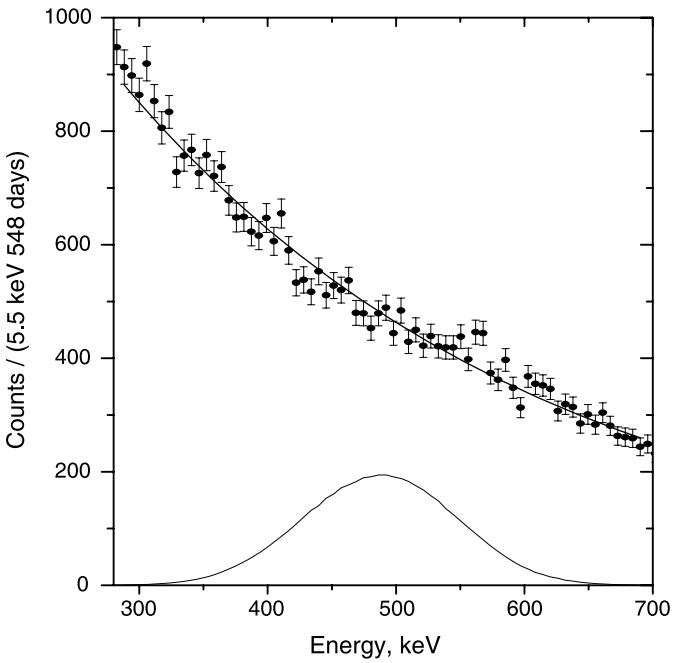

Fig. 7. The exponential fit in the region 290–700 keV. The response function $S_{\rm AE}$ for axio-electric effect corresponds to 5×10^3 events

fine energy scale and resolution parameter, while underlying background described by an exponential function is uncorrelated with these parameters. The fitting of the experimental data with $S_{\rm Model}+S_{\rm Axion}$ was performed in the wider region (73–650) keV. This allowed to fix the energy scale. The upper limit on the number of events was established studying the likelihood function in the more stringent region around expected peak (278–650) keV. The upper limit obtained in this way is stronger than one that can be obtained fitting the data in the (278–650) keV region with $S_{\rm exp}+S_{\rm Axion}$ (without ^{14}C) despite of the larger number of parameters, because the slope of the exponential underlying background is limited by the tail of the ^{14}C beta-spectrum. On the other hand this limit is weaker than one obtained in the total energy region (73–650) keV. The axion response functions have pronounced feature only in the "exponential" region, thus it is natural to follow the χ^2 deviation only in this region in order to define confidence level on the possible admixture of axion interactions.

The results of the fit for the case of axio-electric effect ($S_{\rm AE}(E)$ response) are shown in Fig. 7 (only the region around 478 keV peak is shown). No statistically significant deviations from zero were found for intensities of all response functions. The upper limit on the number of events in the response function (S) was determined by the standard method – $\chi^2_{\rm min}(S)$ profile was calculated for various fixed S values by varying other free parameters.

6 Results and discussions

No positive signal from axion interactions have been found. The upper limits on the number of axion events for four investigated reactions are presented in Table 1. The limits are given for the complete CTF volume and the detection efficiency is taken into account.

6.1 Limits on g_{Ae} and g_{AN} couplings

The number of expected events due to Compton conversion and axio-electric effect in the detector containing N electrons (or ^{12}C nuclei) obtained during time of measurement T are:

$$S=\eta\cdot\Phi_\nu(^7{\rm Be})(\omega_A/\omega_\gamma)\cdot N\cdot T\cdot\sigma_{\rm CC,AE}\,. \qquad (25)$$

The relation obtained in experiment, $S\le S_{\rm lim}$, puts limits on the region of possible values of g_{Ae}, g_{AN} and m_A in assumption that $g_{A\gamma}$ is small enough to not take into account in-flight decay $A\to 2\gamma$. For all axion processes we will consider 3 cases: 1) g_{Ae} and g_{AN} are free unknown parameters, the amplitude of axion reactions depend on m_A only via kinematical factor; 2) g_{Ae} is unknown parameter, g_{AN} depends on axion mass as in KSVZ (or DFSZ) model; 3) g_{Ae} and g_{AN} depends on axion mass as in KSVZ (or DFSZ) model. The results obtained with approach 1) are applicable to any pseudoscalar particle emitted in the nuclear magnetic transitions.

Using expressions for branching ratio (ω_A/ω_γ) (8) and for Compton cross section $\sigma_{\rm CC}$ (14) one can obtains the upper limits on value $(g^0_{AN}+g^3_{AN})^2\cdot g^2_{Ae}$ as a function of axion mass. These model independent limits, which are taking into account only phase space contribution, are shown in Fig. 8. The limit practically does not depend on axion mass in the region $m_A<100$ keV: $|g^0_{AN}+g^3_{AN}|\cdot g_{Ae}\le 1.0\times10^{-10}$. The limit is valid for $g_{Ae}<4\times10^{-7}$, in other case axions are absorbed in the Sun.

In the KSVZ axion model the branching ratio (ω_A/ω_γ) can be calculated as a function of axion mass taking into account the dependencies g^0_{AN} and g^3_{AN} on m_A given by (5) and (6). The region of restricted values of parameters g_{Ae} and m_A are shown in Fig. 9 in comparison with results of experiments with an artificial source ^{65}Zn [33]. The circle shows the upper limit on g_{Ae} obtained for standard axion ($m_A=150$ keV). The limit on parameters g_{Ae} and g_{AN} obtained in [33] can be presented as $|1.8g^0_{AN}+$

Table 1. The upper limits on the number of axion interactions in CTF (counts/548 days). CC – Compton axion to photon conversion $A+e\to e+\gamma$, AE – axio-electric effect $A+e+Z\to e+Z$, PC – Primakoff conversion on nuclei $A+{}^{12}{\rm C}\to\gamma+{}^{12}{\rm C}$. All limits are given at 90% c.l.

reaction	CC	AE	$A\to2\gamma$	PC
$S_{\rm lim}$	180	270	190	165

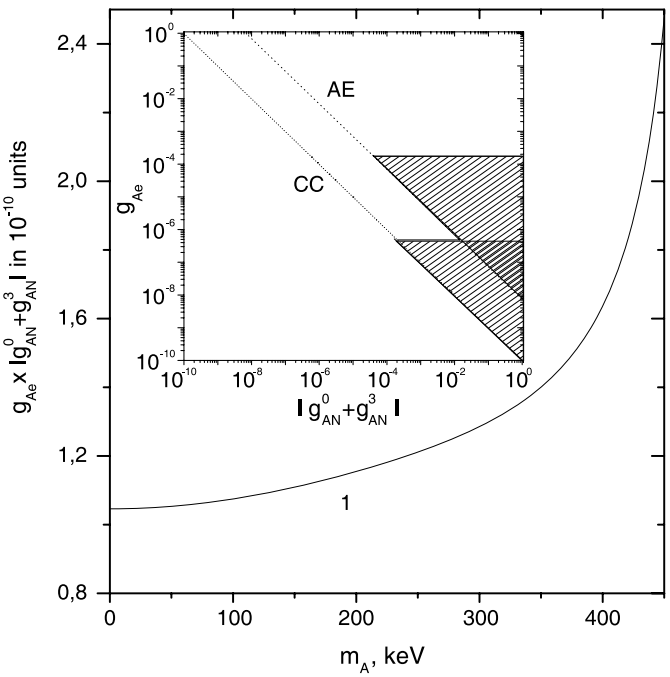

Fig. 8. The upper limits imposed by the Compton production on the $|g^0_{AN}+g^3_{AN}|\cdot g_{Ae}$ versus m_A (values above *line* 1 are excluded). In the *inset* the exclusion plot of g_{Ae} versus $|g^0_{AN}+g^3_{AN}|$ are shown for relations $|g^0_{AN}+g^3_{AN}|\cdot g_{Ae}\le1.0\times10^{-10}$ and $|g^0_{AN}+g^3_{AN}|\cdot g_{Ae}\le9.0\times10^{-9}$ obtained for Compton process and axio-electric effect if $m_A<100$ keV

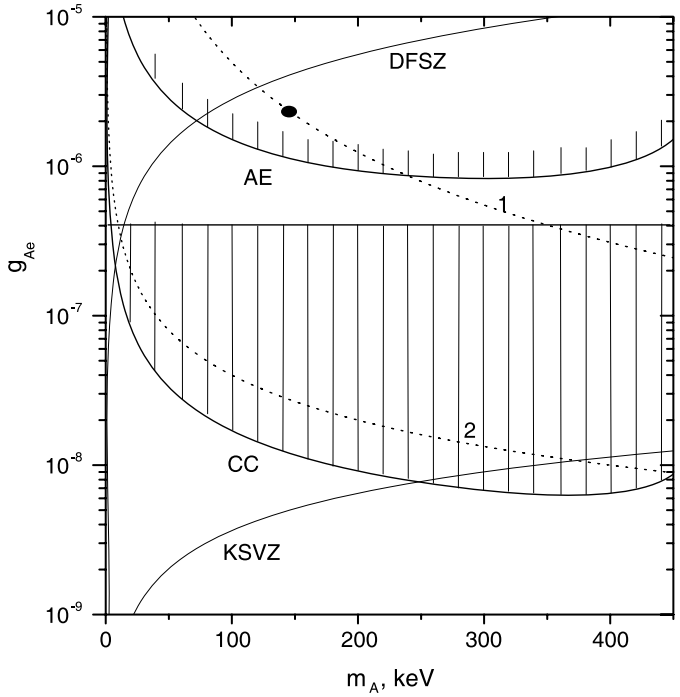

Fig. 9. The exclusion region in g_{Ae} vs. m_A obtained with CTF data for the case of Compton conversion (*shaded area* CC) and axio-electric effect (above *line* AE). *Line* 1 and 2 show the upper limits on g_{Ae} obtained with ^{65}Zn-axions [33] and axions from nuclear reactor [59]. DFSZ and KSVZ predictions are also shown. The *straight line* at $g_{Ae} = 4 \times 10^{-7}$ corresponds to the level of axion absorption

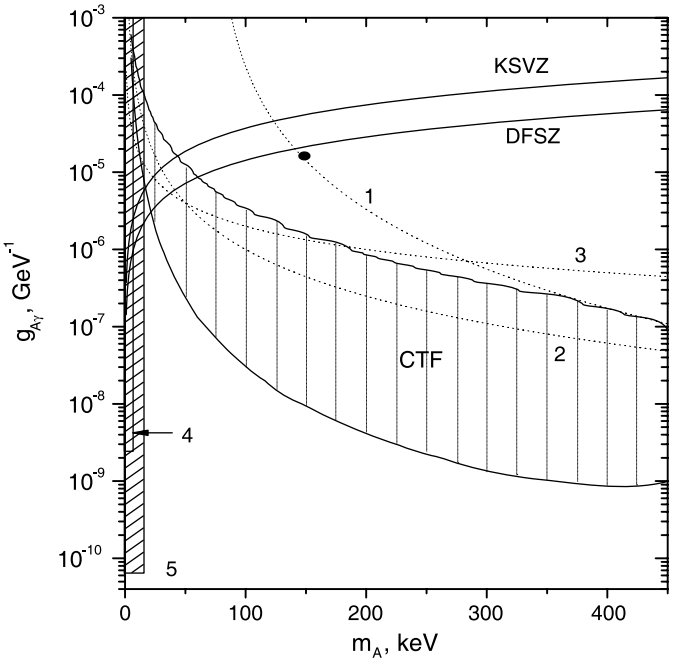

Fig. 10. The exclusion region in $g_{A\gamma}$ vs. m_A imposed by $A \to 2\gamma$ decay with $(g^0_{AN} + g^3_{AN})$ calculated for KSVZ model (CTF *shaded area*). The decay in-flight of the axion is taken into account. 1 – the upper limits on $g_{A\gamma}$ obtained with ^{65}Zn-axions [33], 2 – limits from 2.2 MeV reactor axions decay [60], 3 – limits from Primakoff conversion of reactor axions [59], 4 – limits from coherent conversion in crystal detectors (valid if $m_A < 1$ keV) [23–25], 5 – the most restrictive astrophysical constraint from globular-cluster stars (valid if $m_A < 10$ keV) [10]

$g^3_{AN}| \cdot g_{Ae} \leq 3 \times 10^{-7}$ (line 1). The values of g_{Ae} expected in DFSZ model with $\cos^2\beta = 1$ and in KSVZ model (due to radiative corrections) are shown in the same figure. One can see that our new limit $g_{Ae} < 10^{-8}$ for axions with masses $(100 - 450)$ keV is more than two orders of magnitude stronger than expected in the DFSZ model and restricts the part of allowed region given by theoretical models with heavy axions [11, 12].

Using the relation between g_{Ae} and m_A for the DFSZ model and assuming that $\cos^2\beta = 1$ is, the upper limit on axion mass $m_A \leq 6.3$ keV.

The most stringent limits on g_{Ae} come from astrophysical observation: globular-cluster stars yield the constraint $g_{Ae} \leq 0.5 \times 10^{-12}$ but it is applicable only if $m_A < 10$ keV [61].

The upper limits on the number of events due to axio-electric effect imposes the limit on the value $|g^0_{AN} + g^3_{AN}| \cdot g_{Ae} \leq 9.0 \times 10^{-9}$ for $m_A < 100$ keV. The limit is about 2 orders of magnitude weaker than one given by Compton production, but if Compton process is absent the limit is valid for $g_{Ae} < 1.1 \times 10^{-4}$ (Figs. 8 and 9).

6.2 Limits on $g_{A\gamma}$ and g_{AN} couplings

The analysis of $A \to 2\gamma$ decay and Primakoff photoproduction is more complicated because axions can decay during their flight from the Sun. The exponential dependence of axion flux versus $g_{a\gamma}$ and m_A given by (20) have to be taken into account. For $A \to 2\gamma$ decay the excluded region of parameters $g_{a\gamma}$ and m_A is shown in Fig. 10. The upper and lower lines are obtained for value $S_{\rm lim}(A \to 2\gamma)$ from table 1. For higher values of $g^2_{A\gamma} m^3_A$ axions decay before they reach the detector, for lower $g^2_{A\gamma} m^3_A$ the probability of axion decay inside CTF is too low. The region between lines is excluded. The upper limits on $g_{A\gamma}$ obtained in [33, 59] are shown again. One can see that the CTF limits are more then one order magnitude stronger than obtained by laboratory-based experiments using nuclear reactors. Also the excluded region is new for heavy axions [11, 12].

If axion–photon coupling depends on axion mass as in KSVZ model (17) we exclude axions with mass (15–45) keV (see Fig. 4). The similar restrictions is obtained for DFSZ axion in the case of $\cos^2\beta = 1$.

Considering g_{AN} as a free unknown parameter one can obtain the excluded regions of $g_{a\gamma}$ and g_{AN} for various m_A (Fig. 11). Again, the excluded regions are limited by upper and lower lines corresponding to the fast and the slow decay of axions.

The results of analysis of Primakoff conversion are shown in Fig. 12. Because the number of expected events is proportional to $g^2_{A\gamma} \exp(-g^2_{A\gamma} m^3_A)$ against $g^2_{A\gamma} m^3_A \exp(-g^2_{A\gamma} m^3_A)$ as for $A \to 2\gamma$, search for Primakoff con-

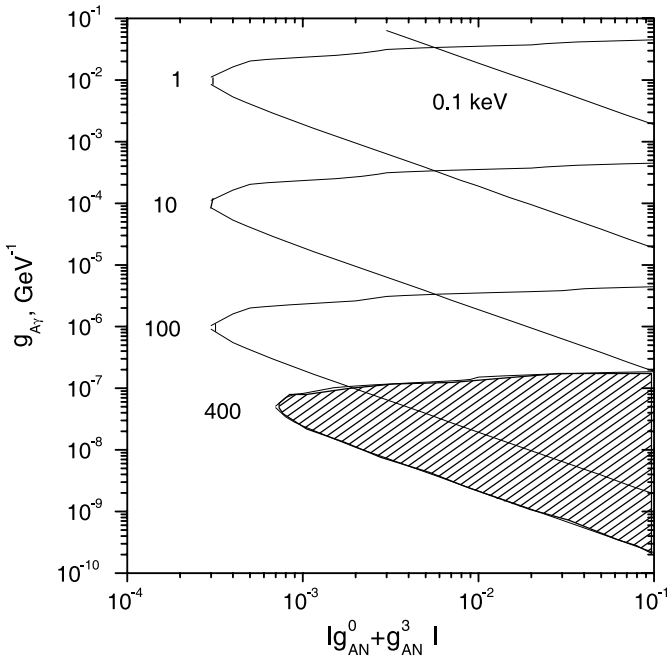

Fig. 11. $A \to 2\gamma$ decay. The excluded regions of $g_{A\gamma}$ and g_{AN} values obtained for different axion masses

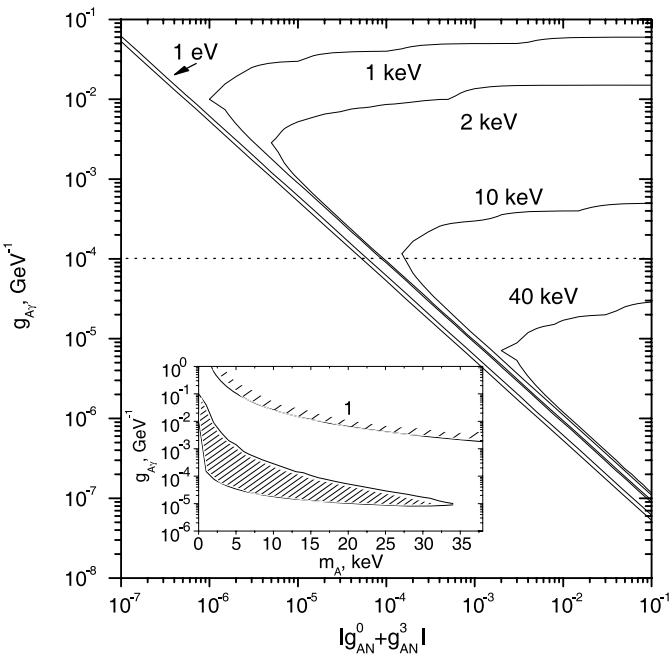

Fig. 12. Primakoff conversion process on ^{12}C. Parameters $g_{a\gamma}$ and g_{AN} are excluded inside outlined regions. In *inset* the excluded region of $g_{A\gamma}$ and m_A is shown (1 – limits from [33])

version is not sensitive to large values of m_A. The model independent limit is $|g^0_{AN} + g^3_{AN}| \cdot g_{A\gamma} \leq 5 \times 10^{-9}$ if $m_A <$ 10 keV. The exclusion plot of $g_{A\gamma}$ versus m_A is shown in inset to Fig. 12. The axion with mass in the region (24–35) keV is excluded in KSVZ axion model. The restrictions on $g_{A\gamma}$ is valid if $g_{A\gamma} < 1 \times 10^{-4}$ (the dotted line on Fig. 12).

7 Conclusions

The search for solar axions emitted in the 478 keV M1-transition of ^{7}Li has been performed with the CTF prototype of Borexino detector. The Compton conversion of axion to a photon, axio-electric effect, decay axion in two photons and Primakoff conversion on nuclei were searched. The signature of all above reactions is the appearance of 478 keV peak in the energy spectra of CTF. No statistical significant indications on axion interactions were found. The new, model independent, upper limits on constants of interaction of axion with electrons, photons and nucleons – $g_{Ae}g_{AN} \leq (1.0\text{–}2.4) \times 10^{-10}$ at $m_A \leq 450$ keV and $g_{A\gamma}g_{AN} \leq 5 \times 10^{-9}$ GeV^{-1} at $m_A \leq 10$ keV were obtained (90%c.l.). For heavy axions the limits $g_{Ae} < (0.7\text{–}2.0) \times 10^{-8}$ and $g_{A\gamma} < 10^{-9}\text{–}10^{-8}$ at $100 < m_A < 400$ keV are obtained in assumption that g_{AN} depends on m_A as for KSVZ axion model. These limits are (2–100) times stronger than obtained by laboratory-based experiments using nuclear reactors and artificial radioactive sources and put some restrictions for heavy axion models.

Acknowledgements. This work was supported by RFBR Grant 02-4-17097, by the NSF Grant 9972127, deutsche Forschungsgemeinschaft (DFG) with the "Sonderforschungsbereich Astroteilchen Physik (SFB375)", the BMBF, and the INFN.

References

1. R.D. Peccei, H. Quinn, Phys. Rev. Lett. **38**, 1440 (1977)
2. R.D. Peccei, Phys. Rev. D **16**, 1791 (1977)
3. S. Weinberg, Phys. Rev. Lett. **40**, 223 (1978)
4. F. Wilczek, Phys. Rev. Lett. **40**, 279 (1978)
5. Particle Data Group, W.M. Yao et al., J. Phys. G **33**, 1 (2006) (URL: http://pdg.lbl.gov)
6. J.E. Kim, Phys. Rev. Lett. **43**, 103 (1979)
7. M.A. Shifman, A.I. Vainstein, V.I. Zakharov, Nucl. Phys. B **166**, 493 (1980)
8. A.R. Zhitnitsky, Yad. Fiz. **31**, 497 (1980)
9. M. Dine, W. Fischler, M. Srednicki, Phys. Lett. B **104**, 199 (1981)
10. G.G. Raffelt, Stars as Laboratories for Fundamental Physics (Univ. of Chicago Press, Chicago, 1996)
11. Z. Berezhiani, L. Gianfagna, M. Giannotti, Phys. Lett. B **500**, 286 (2001)
12. L.J. Hall, T. Watari, Phys. Rev. D **70**, 115 001 (2004)
13. P. Sikivie, Phys. Rev. Lett. **51**, 1415 (1983)
14. P. Sikivie, Phys. Rev. D **32**, 2988 (1985)
15. L. Krauss, J. Moody, F. Wilczek et al., Phys. Rev. Lett. **55**, 1797 (1987)
16. K. van Bibber et al., Phys. Rev. D **39**, 2089 (1989)
17. W. Wuensch, S. De Panfilis-Wuensch, Y.K. Semertzidis et al., Phys. Rev. D **40**, 3153 (1989)
18. C. Hagmann, D. Kinion, W. Stoeffl et al., Phys. Rev. Lett. **80**, 2043 (1998)
19. M. Muck, J.B. Kycia, J. Clarke, Appl. Phys. Lett. **78**, 967 (2001)
20. D. Lazarus, G. Smith, R. Cameron et al., Phys. Rev. Lett. **69**, 2333 (1992)

21. Y. Inoue, T. Namba, S. Moriyama et al., Phys. Lett. B **536**, 18 (2002)
22. CAST Collaboration, K. Zioutas et al., Phys. Rev. Lett. **94**, 121 301 (2005)
23. F.T. Avignone et al., Nucl. Phys. Proc. Suppl. **72**, 176 (1999)
24. R. Bernabei, P. Belli, R. Cerulli et al., Phys. Lett. B **515**, 6 (2001)
25. A. Morales et al., Astropart. Phys. **16**, 325 (2002)
26. W.C. Haxton, K.Y. Lee, Phys. Rev. Lett. **66**, 2557 (1991)
27. S. Moriyama, Phys. Rev. Lett. **75**, 3222 (1995)
28. M. Krčmar, Z. Krecak, M. Stipcevi et al., Phys. Lett. B **442**, 38 (1998)
29. K. Jakovcic, Z. Krecak, M. Krčmar et al., nucl-ex/0402016 (2004)
30. C.M. Lederer, V.S. Shierley, Table of Isotopes (Wiley, New York, 1978)
31. J.N. Bahcall, A.M. Serenelli, S. Basu, Astrophys. J. **621**, L85 (2005)
32. T.W. Donnelly et al., Phys. Rev. D **18**, 1607 (1978)
33. F.T. Avignone III et al., Phys. Rev. D **37**, 618 (1988)
34. M. Krčmar et al., Phys. Rev. D **64**, 115 016 (2001)
35. A.V. Derbin et al., JETP Lett. **81**, 365 (2005)
36. Borexino Collaboration, H.O. Back et al., Phys. Lett. B **525**, 29 (2002)
37. Borexino Collaboration, H.O. Back et al., Phys. Lett. B **563**, 35 (2003)
38. Borexino Collaboration, H.O. Back et al., Phys. Lett. B **563**, 23 (2003)
39. Borexino Collaboration, H.O. Back et al., JETP Lett. **78**, 261 (2003)
40. Borexino Collaboration, H.O. Back et al., Eur. Phys. J. **37**, 421 (2004)
41. A.V. Derbin, O.J. Smirnov, JETP Lett. **76**, 409 (2002)
42. M. Srednicki, Nucl. Phys. B **260**, 689 (1985)
43. D.B. Kaplan, Nucl. Phys. B **260**, 215 (1985)
44. V. Mateu, A. Pich, JHEP **10**, 41 (2005)
45. R. Mayle et al., Phys. Lett. B **219**, 515 (1989)
46. G.K. Mallot, Int. J. Mod. Phys. A **15**, 521 (2000) Supp01B
47. J. Engel, D. Seckel, A.C. Hayes, Phys. Rev. Lett. **65**, 960 (1990)
48. M.S. Turner, Phys. Rep. **197**, 67 (1990)
49. A.R. Zhitnitsky, Y.I. Skovpen, Yad. Fiz. **29**, 995 (1979)
50. J.N. Bahcall, M.H. Pinsonneault, S. Basu, Astrophys. J. **555**, 990 (2001)
51. Borexino Collaboration, G. Alimonti et al., Astropart. Phys. **18**, 1 (2002)
52. Borexino Collaboration, G. Alimonti et al., Nucl. Instrum. Methods A **406**, 411 (1998)
53. Borexino Collaboration, H.O. Back et al., physics/0408032 (2004)
54. Borexino Collaboration, G. Alimonti et al., Phys. Lett. B **422**, 349 (1998)
55. Borexino Collaboration, G. Alimonti et al., Astropart. Phys. **8**, 141 (1998)
56. Borexino Collaboration, G. Alimonti et al., Nucl. Instrum. Methods A **440**, 360 (2000)
57. W.R. Nelson, H. Hirayama, D.W.O. Rogers, The EGS4 code system, SLAC-265 (1985)
58. O.J. Smirnov, Instrum. Exp. Technol. **46**, 327 (2003)
59. H.M. Chang et al., hep-ex/0609001v1, v2 (2007)
60. S.N. Ketov et al., JETP Lett. **44**, 146 (1986)
61. G.G. Raffelt, A. Weiss, Phys. Rev. D **51**, 1495 (1995)